Journal of Hazardous Materials 416 (2021) 126240

Contents lists available at ScienceDirect

Journal of Hazardous Materials

journal homepage: www.elsevier.com/locate/jhazmat

Phosphate controls uranium release from acidic waste-weathered Hanford sediments

Angélica Vázquez-Ortega [a,b,*], Nicolas Perdrial [a,c], Estela Reinoso-Maset [d,e], Robert A. Root [a], Peggy A. O'Day [d,f], Jon Chorover [a]

[a] Department of Environmental Science, University of Arizona, 1177 East Fourth Street, Tucson, ARI 85721, USA
[b] School of Earth, Environment and Society, Bowling Green State University, 190 Overman Hall, Bowling Green, OH 43403, USA
[c] Department of Geology, University of Vermont, 180 Colchester Avenue, Burlington, VT 05405, USA
[d] Sierra Nevada Research Institute, University of California Merced, 5200 North Lake Road, Merced, CA 95343, USA
[e] Centre for Environmental Radioactivity CoE, Faculty of Environmental Sciences and Natural Resource Management, Norwegian University of Life Sciences, 1432 Aas, Norway
[f] Life and Environmental Sciences Department, School of Natural Sciences, University of California - Merced, 5200 North Lake Road, Merced, CA 95343, USA

ARTICLE INFO

Editor: Dr. L. Haizhou

Keywords:
Uranium minerals
Phosphate
Flow-through columns
Mineral transformation
Hanford site

ABSTRACT

Mineral dissolution and secondary phase precipitation may control the fate of inorganic contaminants introduced to soils and sediments during liquid waste discharges. When the solutions are aggressive enough to induce transformation of native minerals, incorporated contaminants may be released during dissolution due to percolation of meteoric waters. This study evaluated the release of uranium (U) from Hanford sediments that had been previously reacted for 180 or 365 days with liquid waste solutions containing U with and without 3 mM dissolved phosphate at pH 2 and 3. Flow-through column experiments were conducted under continuous saturated flow with a simulated background porewater (BPW; pH ~7) for 22 d. Up to 5% of the total U was released from the sediments reacted under PO_4-free conditions, attributable to the dissolution of becquerelite and boltwoodite formed during weathering. Contrastingly, negligible U was released from PO_4-reacted sediments, where meta-ankoleite was identified as the main U-mineral phase. Linear combination fits of U L_{III}-edge EXAFS spectra of sediments before and after BPW leaching and thermodynamic calculations suggest that the formed becquerelite and meta-ankoleite transformed into schoepite and a phosphuranylite-type phase, respectively. These results demonstrate the stabilization of U as recalcitrant uranyl minerals formed in sediments and highlight the key role of PO_4 in U release at contaminated sites.

1. Introduction

Nuclear weapons production activities between the 1940's and 1980's at the Hanford Site (WA, USA) left a legacy of high-level radioactive and non-radioactive waste in subsurface sediments that continues to pose high health risks to humans and ecosystems. Facilities in the 200 Hanford Area were employed to reprocess uranium (U) and plutonium (Pu) from irradiated fuel rods (Zachara et al., 2007) and about 1.7 billion m^3 of liquid waste were discharged to the vadose and saturated zones in this area (CH2M HILL, 2006; 2010). Engineered surface "Crib" structures located in the 200 Hanford Area received hazardous and radioactive waste between 1952 and 1988. Soil characterization in the vadose zone beneath the 216-U-8 and 216-U-12 Cribs revealed U contamination in the soil profile (DOE, 2010). These Cribs received approximately 378 * 10^3 and 150 * 10^3 m^3 of U contaminated waste, respectively. The U(VI) geochemical behavior in the vadose zone beneath these Cribs has been postulated to be controlled by sediment composition, waste-water composition during the active years, and pore water composition after cessation of waste disposal (Zachara et al., 2007). The original chemical composition and pH of the wastewater discarded in the 216-U-8 and 216-U-12 Cribs is unknown, but estimated compositions, including proton activity, have been inferred based on the Hanford soil inventory model (Corbin et al., 2005; CH2MHILL, 2006), suggesting that the Cribs principally received acidic (pH 2–3) waste solutions.

Uranium wastes in the vadose zone at the 200 Hanford Area have

* Corresponding author at: School of Earth, Environment and Society, Bowling Green State University, 190 Overman Hall, Bowling Green, OH 43403, USA.
E-mail address: avazque@bgsu.edu (A. Vázquez-Ortega).

https://doi.org/10.1016/j.jhazmat.2021.126240
Received 21 December 2020; Received in revised form 27 April 2021; Accepted 24 May 2021
Available online 27 May 2021
0304-3894/Published by Elsevier B.V.

been investigated by subsurface sampling and microscale investigations (Catalano et al., 2004; Christensen et al., 2004; McKinley et al., 2007; Um et al., 2009). Precipitation and characterization of uranyl (UO_2^{2+}) solid phases using acidic waste simulating the estimated chemical composition discharged at the Hanford site have been previously conducted to study the U(VI) partitioning and mineral transformations that may have occurred during the disposal of high-level radioactive and non-radioactive waste (Kanematsu et al., 2014; Mehta et al., 2014, 2015; Gartman et al., 2015; Wang et al., 2017; Perdrial et al., 2018). Homogeneous nucleation experiments using synthetic acidic to circumneutral waste solutions spiked with dissolved silica (as expected from silicate dissolution reactions) revealed the formation of compreignacite [$K_2(UO_2)_6O_4(OH)_6 \cdot 7\ H_2O$] and boltwoodite [$K(UO_2)_2O_4(HSiO_4)_2 \cdot 0.5\ H_2O$] and, in presence of phosphate, meta-ankoleite [$K(UO_2)(PO_4) \cdot 4\ H_2O$] (Kanematsu et al., 2014). These U-mineral phases, together with becquerelite [$Ca(UO_2)6\ O_4(OH)_6 \cdot 8\ H_2O$], were also detected after acidic weathering of uncontaminated Hanford sediments using batch reactors or flow-through columns (Mehta et al., 2014; Gartman et al., 2015; Pan et al., 2016; Perdrial et al., 2018). Nevertheless, the contemporary geochemical processes governing the transformation and transport of U(VI) in the 200 Hanford Area sediments impacted by acidic waste solutions are not well understood.

The present study aimed to evaluate the release of U(VI) from acidic waste weathered Hanford sediments. Leaching experiments were conducted in a flow-through column set-up at a continuous, uniform flow using a simulated circumneutral Hanford background porewater (BPW) solution representing the infusion of meteoric waters. These flow-through column experiments were carried out using Hanford sediments that had previously been weathered in the laboratory for 180 and 365 d with acidic U(VI)-containing solutions at pH 2 and 3 to simulate the acidic high-level radioactive waste discharged into the 216-U-8 and 216-U-12 Cribs during active periods at the Hanford site. Results on effluent porewater were then used in combination with data from sequential chemical extractions, thermodynamic modeling, and extended X-ray absorption fine structure (EXAFS) spectroscopy of the materials before and after leaching to assess the impact of U(VI) solid phase speciation on the subsequent U release from the sediments. The results provide information on the potential fate of U(VI) released to the vadose zone beneath the 216-U-8 and 216-U-12 Cribs (within the experimental conditions constraints). Although the precise composition of the liquid waste introduced to the Cribs is subject to uncertainty, available data from Corbin et al. (2005) was used to design a range of liquid waste conditions that will allow to improve our understanding on geochemical controls over U transport and enhance remediation efficiency at the Hanford Site.

2. Material and methods

2.1. Acidic waste weathered sediments

Acidic waste-weathered sediments were generated by reacting uncontaminated Hanford sediments with acidic U(VI)-containing synthetic waste solutions simulating those disposed in the 216-U-8 and 216-U-12 Cribs at the 200 Hanford Area (Perdrial et al., 2018). Detailed description of the experimental parameters is found in Perdrial et al. (2018). Although the chemical composition of the different types of waste discharged into the Cribs was not reported precisely during activity, it has been simulated by the Hanford Soil Inventory Model (SIM) (Corbin et al., 2005). The SIM identified three distinct solution compositions representative of the main waste streams: spent nitric acid (SNA), dilute and concentrated uranium nitrate hexahydrate (UNH), and mixed solutions. The pH of the streams is not known, but the largest volume of waste was composed of UNH and SNA, thus it is expected to be highly acidic, yet somewhat neutralized by the mixed solutions. Moreover, the SIM data suggest 2.8 mM PO_4 in the UNH streams, whereas none is predicted for SNA. Therefore, pH values of 2 and 3 and phosphate concentration values of 0 and 3 mM were chosen to assess the effects of these parameters during sediment-waste weathering reactions (Perdrial et al., 2018).

Uncontaminated Hanford sediments collected at the 218-E-12B Burial Ground excavation site (Riley and Zachara, 1992) were reacted at a solid to solution ratio (by mass) of 1:50 with simulated waste solutions of the following composition (all in millimolal units): 100 K^+, 0.75 Na^+, 2.00 Cl^-, 100 NO_3^-, 0.86 U, and 0.0 or 3.0 PO_4^{3-} at pH 2 or 3. The pH was adjusted at the beginning of the experiment using concentrated HNO_3 and monitored through the reaction period with a gel-filled electrode to avoid contamination from the KCl filling solution (VWR sympHony). After 180 and 365 d, the acidic waste-weathered Hanford sediments were washed twice in 90% ethanol, once in a 30/70 (w/w) ethanol/water mix, and once with 100% ultrapure (18 MΩ·cm) water. These three liquid washes enabled full removal of entrained solution while minimizing the need for prolonged contact with aggressive (*i.e.*, low ionic strength) water prior to the dissolution experiments. Washed weathered sediments were subsequently freeze-dried ($< 133 \times 10^{-3}$ mbar), homogenized and stored at room temperature (as described in Thompson et al., 2010).

Bulk acidic waste-weathered sediments were used in the sequential chemical extractions and the flow-through column dissolution experiments, whereas isolated subsamples of the sediment fine fraction were used for detailed post-reaction investigations. For the fine fraction separation, bulk sediments (*ca.* 300 mg) were suspended in ethanol followed by sonication for 8 min. Particles remaining in suspension 2 min after sonication were aspirated by pipette and dried at 25 °C for 12 h. The residual bulk material with fine fraction removed was discarded. This method was selected over the classical separation by centrifugation to reduce the reaction time in an aqueous liquid phase and isolate more than 90% of the particles with <50 μm in equivalent spherical diameter, as shown by Perdrial et al. (2011, 2014).

2.2. Sequential Chemical Extractions

Bulk acidic waste-weathered sediments (1.0 g, freeze-dried) were subjected to a four-step sequential extraction (SE) scheme (Table 1; adapted from McKeague and Day, 1966; Begin and Fortin, 2003; Dold,

Table 1
Sequential extraction procedure (including mass ratio, extraction pH and temperature, shaking time) applied to the bulk acid-waste weathered Hanford sediments used in this work and the corresponding targeted phase pools. Each extraction step (except for step 1) was followed by a rinse with ultrapure water (18.2 MΩ·cm) for 20 min with a 1:20 solid to solution mass ratio at room temperature (RT). The procedure was adapted from McKeague and Day, 1966; Begin and Fortin, 2003; Dold, 2003; Zhou and Gu, 2005; and Chorover et al., 2008.

Step	extraction	Procedure
1	Water (targeting readily solubilized forms)	Nanopure water 18.2 MΩ·cm Adjust pH to 7.0 1:40 g/g Shake for 1 h at RT
2	Bicarbonate solution (targeting adsorbed U and uranyl phosphate, oxyhydroxide, silicate, and sulfate minerals)	1 M $NaHCO_3$ Adjust pH to 8.6 1:20 g/g Shake for 7 d at RT
3	Acidic ammonium oxalate (targeting poorly crystalline Al and Fe oxides)	0.2 M $(NH_4)_2C_2O_4 \cdot H_2O$ Adjust pH to 3 with 0.2 M oxalic acid 1:40 g/g Shake for 4 h at RT in darkness
4	Nitric acid digestion (targeting recalcitrant U and P minerals)	Microwave assisted acid digestion 1:3 molar ratio of HCl/HNO_3 EPA METHOD 3050B

2003; Zhou and Gu, 2005; and Chorover et al., 2008). This SE scheme resulted in five chemically distinct U pools targeting the water-soluble U and P species (step 1), bicarbonate soluble phosphates, silicates and (oxy)hydroxides (step 2), oxalate extractable poorly crystalline Al and Fe oxides (step 3), and acid soluble minerals (step 4). The residual fraction represents mainly crystalline silicates. Each extraction step (except for step 1) was followed by a wash with ultrapure water (18.2 MΩ·cm) for 20 min at 1:20 solid to solution mass ratio at room temperature. Extractions and rinses were shaken at 100 rpm followed by centrifugation at 18,500 relative centrifugal force (RCF) for 20 min and filtered through a 0.2 μm acid washed cellulose acetate membranes. The rinses were combined with the corresponding extraction supernatant solutions and the remaining solids were subjected to further extraction. Extractions were performed in triplicate. Furthermore, sediment-free controls ('blanks') were carried out in triplicate in parallel to the sediment samples. Concentrations detected from the blanks were subtracted from the sediment samples at each extraction step.

Supernatant solutions from the sequential extractions were analyzed for U, P, Si, Fe, Al, Mn, Mg, K, Ca by inductively coupled plasma mass spectrometry (Perkin Elmer Elan DRC II ICP-MS Waltham, MA) (details in Section 2.4 and the SI). Element concentrations were used to calculate the extracted fraction at each step and compared to the initial total element concentrations measured by XRF (details in Section 2.4 and the SI). Uncertainties associated with the XRF measurements and the sequential chemical extraction procedure may have resulted in small discrepancies in the total element concentrations, thus leading in some cases to slightly higher (overestimation) or lower (underestimation) than 100% on the total extracted fractions but all were within an acceptable ±2–5%.

2.3. Flow-through column experiments

Duplicate polypropylene columns of 2.0 cm^3 total volume (3.2 cm length, 0.9 cm diameter) were packed with freeze-dried acidic waste-weathered sediments to an average bulk density (ρ_b) of 1.4 g cm^{-3} and stored in the dark until experiments were performed. Polytetrafluoroethylene (PTFE) frits (of 20 μm pore size) were placed at the bottom and top of the column. A 13 mm diameter hydrophilic filter with a pore size of 0.45 μm (GHP, Life Sciences) was placed at the outlet of the column to avoid the loss of fine silt and clay particles. The porosity was determined as $1 - (\rho_b / \rho_s)$ using an assumed particle density (ρ_s) of 2.65 g cm^3.

Column influent solution consisted of a synthetic background porewater (BPW) solution characteristic of the Hanford site (Thompson et al., 2010). Final solution millimolality (mmol kg^{-1}) was: 3.7 Na^+, 0.3 K^+, 2.7 Ca^{2+}, 1.0 Mg^{2+}, 1.0 CO_3^{2-}, 1.7 SO_4^{2-}, 7.9 Cl^- at pH 7.2. The pH was adjusted at the beginning of the experiment using concentrated HNO_3. The BPW solution was delivered to the columns using PTFE and polyvinyl chloride tubing and a peristaltic pump (Masterflex L/S) at a constant flow of 0.05 mL min^{-1}, corresponding to a linear velocity of 0.099 cm min^{-1} (full system set-up shown in Fig. S1, Supplemental Information). Upward solution flux through the columns was utilized to diminish preferential flow. Effluent solutions were collected with a fraction collector (Lambda Omnicoll, Lambda Laboratories Instruments, Zurich, Switzerland) with samples collected for every 25-pore volumes (PV, *ca.* 0.8 mL/PV) for the first 500 PV (400 min/sample), and thereafter for every 50 PV (800 min/sample) to a total of *ca.* 2000 PV, *i.e.*, *ca.* 22 d total collection time. A total of 50 samples (*ca.* 1600 mL) were collected for each replicate column. Solution samples were then sealed in polypropylene bottles and refrigerated at 4 °C prior to analysis. Selected samples spread over the course of the experiment were analyzed for pH, dissolved carbonate, anions and metal(loid)s (details in Section 2.4 and the SI). At the end of the leaching period, the residual pore solution was extracted by air displacement and included in the last effluent sample. Effluent volumes were mathematically corrected for any evaporative loss that may have occurred during leaching. Undisturbed columns were freeze-dried and stored prior to solid phase characterization.

2.4. Solid phase and effluent characterization

Solid phase characterizations were performed on ground bulk and fine fraction sediments before (*i.e.*, after acidic-waste weathering) and after the BPW leaching experiments to identify uranyl-mineral phases and elucidate their transformation. Total element concentrations were determined in bulk sediments before (unreacted) and after acidic waste weathering by X-ray fluorescence (XRF). Uranium solid phase speciation in the fine fractions of acidic waste-weathered sediments before and after BPW leaching was determined by linear combination fits (LCF) of U L_{III}-edge extended X-ray absorption fine structure (EXAFS) spectra collected at the Stanford Synchrotron Radiation Lightsource (SSRL). Full details of analytical procedures and data treatment are given in the Supplemental Information.

Effluent solutions were monitored throughout the flow-through column experiments. The pH values were measured using a gel-filled electrode to avoid contamination from the KCl filling solution (VWR sympHony). Aqueous phase concentrations of total inorganic carbon (TIC) were measured using a Shimadzu TOC-VCSH analyzer (Columbia, MD), anions (Cl^-, NO_3^-, SO_4^{2-}, and PO_4^{3-}) were measured by ion chromatography (Dionex DX600, Sunnyvale, CA), and metal(loid)s, including U, Ca, K, Fe, Al, Na, Mg, and Si were measured by ICP-MS. Rhodium (Rh) was added as an internal standard for all ICP-MS analyses, and quality assurance and control protocols were applied during analysis run (details in the Supplemental Information). Results from the column experiments were reported as duplicate means and variance was quantified as 95% confident interval. Therefore, symbols for concentration wherein error bars do not overlap indicate statistically significant differences at the $\alpha = 0.05$ level.

2.5. Thermodynamic modeling

Uranyl aqueous speciation and mineral saturation indices of effluent solutions from the flow-through column experiments were calculated based on measured pH, TIC, anions, cations and metal(loid)s using Geochemist's Workbench (GWB; Version 10, Aqueous Solutions LLC). The GWB default thermodynamic database (thermo.com.v8.r6) was supplemented with internally consistent thermodynamic data for uranyl minerals (*i.e.*, uranyl oxyhydroxide, phosphate, and silicate phases) obtained from the literature (Gorman-Lewis, et al., 2008, 2009; Juillerat et al., 2018; Kanematsu et al., 2014; Reinoso-Maset et al., 2017, 2020). To the authors' knowledge, there are no published experimental solubility constants for the phosphuranylite species [$KCa(H_3O)_3(UO_2)_7(PO_4)_4O_4 \cdot 8\ H_2O$], which was identified as a reaction product contributing to the LCFs to several EXAFS spectra following our column experiments. Juillerat et al. (2018) reported a Gibbs free energy of formation of −6685 KJ mol^{-1} for $K_4[(UO_2)_3O_2(PO_4)_2]$, a member of the phosphuranylite group (Lussier et al., 2016), estimated using single-ion additive methods coupled with volume-based thermodynamics. We need to emphasize that the phosphuranylite phase identified with EXAFS in our reacted sediments is different from $K_4[(UO_2)_3O_2(PO_4)_2]$ used by Juillerat et al. (2018), because it contains a mixture of K and Ca along with structural H_2O. Therefore, our calculated solubility product ($\log K_{sp} = -32.51$) for $K_4[(UO_2)_3O_2(PO_4)_2]$ based on the reported value for the Gibbs free energy of formation is likely not accurate for our identified phase but nonetheless provides a rough estimate of solubility for members of the phosphuranylite mineral group. Due to the presence of sulfate in the input solution, Mg-zippeite [$Mg_2(UO_2)_6(SO_4)_3(OH)_{10} \cdot H_2O$], a uranyl sulfate mineral phase, was also included in the database. The main uranyl mineral phases considered in the calculations are listed in Table S2 in SI.

Saturation indices of effluent solutions with respect to relevant minerals ($\log \Omega$) were calculated to examine potential mineral solubility

controls on solute behavior over the course of the experiments. The log of the saturation index (*log Ω*) describes quantitatively the relative saturation of an aqueous solution with respect to equilibrium with a solid phase:

$$log\ \Omega = log\ (IAP/K_{SO}) \quad (1)$$

where the ion activity product (*IAP*) is the reaction quotient that includes all measured species activities involved in the mineral dissolution reaction except for solvent water and solids (which are assigned unit activity), and K_{SO} is the thermodynamic mineral solubility product constant. For *log Ω* above (below) zero, the system is oversaturated (undersaturated) with respect to a specific mineral.

3. Results

3.1. Uranium speciation in acidic waste-weathered sediments

The total U and P concentrations measured by XRF showed a significant concentration increase in the acidic waste-weathered Hanford sediments compared to the bulk unreacted materials (Table S1, Supplemental Information; pH 3: Perdrial et al., 2018; pH 2: this study). The presence of PO_4 in the weathering waste solution at pH 2 or 3 (hereafter referred to as "+PO_4" systems) resulted in higher P concentration in the sediments than PO_4-reactant free waste weathering (hereafter referred to as "-PO_4" systems). The reaction time (180 *vs.* 365 d) however did not clearly affect the total concentrations under either weathering conditions. After weathering, 20–100% of U in the simulated waste solution was incorporated into the solid phase (Perdrial et al., 2018).

Analysis of the U L_{III}-edge EXAFS spectra by LCF indicated that the solid phase U speciation in acidic waste-weathered sediments was strongly dependent on the dissolved phosphate concentration and to a lesser extent on the pH and reaction time (Fig. 4 and S7 and Table S3; Perdrial et al., 2018 and this study). In the -PO_4 sediment systems at pH 2, boltwoodite (180 d: 56%, 365 d: 51%), meta-ankoleite (180 d: 51%, 365 d: 55%), and becquerelite (180 d: 21%, 365 d: 18%) were identified as the main uranyl minerals. Compreignacite (180 d: 55%), becquerelite (180 d: 21%), and boltwoodite (180 d: 16%) were detected in the pH 3 systems after 180 d, whereas only compreignacite (65%) and boltwoodite (47%) were detected after 365 d. In the +PO_4 systems at pH 2, meta-ankoleite (180 d: 45%; 365 d: 66%) and boltwoodite (180 d: 43%; 365 d: 49%) were the major phases with a smaller becquerelite (180 d: 21%; 365 d: 13%) contribution. At pH 3, boltwoodite (180 d: 13%; 365 d: 14%) and becquerelite (180 d: 27%; 365 d: 16%) and compreignacite (only at 365 d: 33%) showed similar contribution to the LCF fit, whereas meta-ankoleite was the main phase (180 d: 69%; 365 d: 52%).

Sequential chemical extractions performed on the acidic waste-weathered sediments showed that the largest U mass fractions were extracted with $NaHCO_3$ (targeting U-bearing minerals). In the +PO_4 systems, bicarbonate solution extracted 100% and 97% of the U present in the 180 d and 365 d pH 2 weathered sediments, respectively (Fig. 1A), whereas the corresponding percentage of bicarbonate extractable U from pH 3 weathered sediments was 99% and 103% (Fig. 1D). In the -PO_4 sediment systems, bicarbonate extracted lower fractions of U, *i.e.*, 68% and 91% (pH 2; Fig. 1A) and 75% and 95% (pH 3; Fig. 1D) for 180 and 365 d, respectively.

In the +PO_4 systems at pH 2 reacted for 180 and 365 d, most of the P was extracted by bicarbonate solution (57–59%), and to a lesser extent by oxalate (27–33%), nitric acid (7.6–7.7%) and water (4.4–4.5%) (Fig. 1B). For the +PO_4 systems at pH 3, a higher fraction of P was extractable with bicarbonate (68%), followed by the acid soluble (6–15%), oxalate extractable (10–13%), and water soluble (5–7%) fractions (Fig. 1E). In the -PO_4 systems, extractable bicarbonate fractions for the 180- and 365-d weathered sediments were, respectively, 40% and 28% (pH 2) and 3.4% and 0.75% (pH 3). In all weathered sediments, Si was dominantly associated with the residual pool (Fig. 1C and F). Corresponding sequential extraction data for Fe, Al, Mn, Mg, K, and Ca are presented in Fig. S2 (Supplemental Information). Overall, the largest fractions of Fe, Al, Mg, and Ca were associated with the oxalate extractable and residual pools. In contrast, most Mn was released during the nitric acid extraction (Figs. S2C and S2I), and K was dominantly in the residual pool (Figs. S2E and S2K). Extractable average concentrations (in mmol kg^{-1}) for U and major elements in the bulk acidic waste-weathered Hanford sediments for all systems and the corresponding stoichiometric element ratios can be found in Tables S4-S5 and Table S6 (Supplemental Information), respectively.

3.2. Flow-through column experiments

Flow-through leaching of acidic waste-weathered sediments showed that the effluent solution pH in the +PO_4 systems (pH 2) during the first 800 pore volumes (PV) remained considerably lower (ranging from 3.6

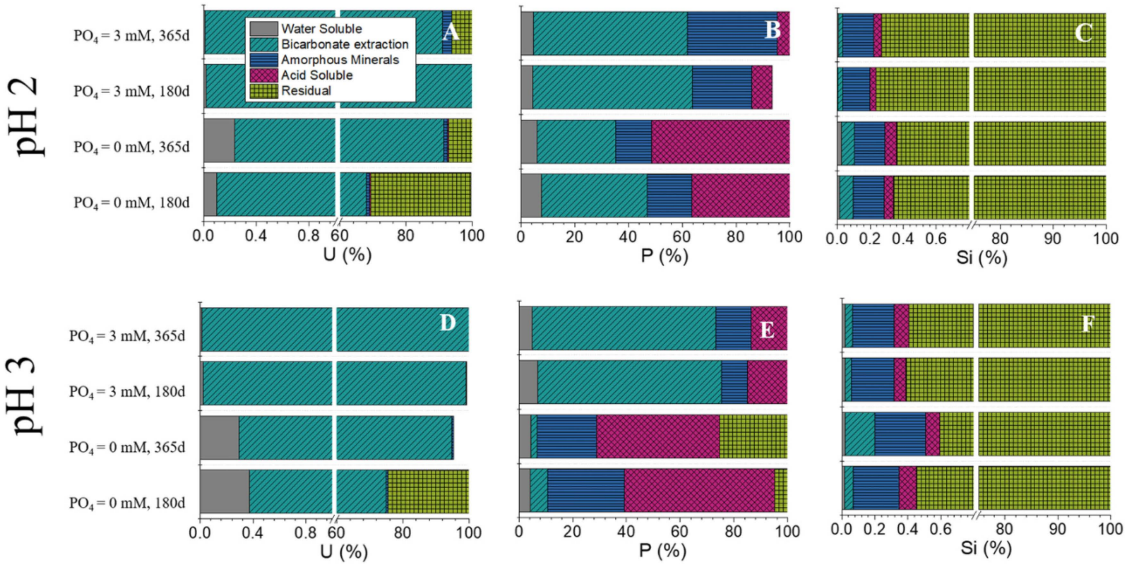

Fig. 1. Uranium (A, D), P (B, E), and Si (C, F) extractability patterns for PO_4–reactant (+PO_4) and PO_4-reactant free (-PO_4) acidic waste-weathered Hanford sediments reacted at pH 2 or 3 for 180 or 365 days. Note that the x-axes represent the fraction (as %) of total element concentration measured in weathered sediments (Table S1) and that U and Si x-axes are broken for clarity of smaller fractions. Data in D, E, and F have been reproduced from Perdrial et al. (2018).

to 6.3) than that of the influent solution (pH 7.2) (Fig. 2A). Even at steady state U release (800–1200 PV), the effluent solution pH was *ca.* 6.5. In the -PO_4 systems (pH 2), effluent pH approached the influent pH more rapidly in the first 800 PV. Between 200 and 1000 PV (pH 2 systems), effluent pH was significantly lower in the +PO_4 than in the -PO_4 systems (95% confident interval). In all systems at pH 3 (except for +PO_4, 180 d), effluent pH was *ca.* 1 unit higher than that of the influent solution for the first 600 PV (Fig. 2G). After *ca.* 800 PV, effluent pH decreased 1 unit relative to the influent solution, except for the +PO_4, 365 d system that remained at pH ~8 (Fig. 2G). Among the pH 3 systems, effluent pH in the +PO_4, 365 d sediments remained distinctly higher than input solution from 800 to 2200 PV. The influent solution contained about 42 μM of HCO_3^-; however, on average, pH 2 weathered sediments in both +PO_4 and -PO_4 systems resulted in lower total carbonate concentrations (*i.e.*, the molar sum of aqueous $H_2CO_3^0$ and HCO_3^- species) in the effluent solutions during the first 400 PV (Fig. 2B). For pH 3 systems, effluent carbonate concentrations were slightly lower than in the influent solution but with large variability (Fig. 2H).

In all +PO_4 systems, negligible U was released, irrespective of weathering pH and time (Fig. 2C–I and Figs. S3B and S3F [Supplemental Information]). In contrast, the -PO_4 systems weathered at pH 2 and 3 for 180 and 365 d released 4–5% of the initial U by the end of the leaching experiment (Figs. S3B and S3F). Phosphorus released from the +PO_4 systems ranged from 15% to 25% (pH 2) to *ca.* 5% (pH 3), whereas in the -PO_4 systems, P release ranged from *ca.* 5% (pH 2) to non-detectable (pH 3), irrespective of weathering time (Fig. 2D–J and Fig. S3 [Supplemental Information]). In both pH 2 and pH 3 systems, P release was significantly higher in the +PO_4 than in the -PO_4 systems before 1200 PV. Silicon release followed similar trends in all systems, with high concentration in the initial leaching stage followed by a decrease with time (Fig. 2E and K). Aluminum mobilization among all treatments was low except for the first PV at pH 2 (Fig. 2F and L).

Evolution of effluent concentrations for major cations, Fe and SO_4 are shown in Fig. S4 (Supplemental Information). In the pH 2 systems (+PO_4 and -PO_4), significant amounts of Na were consistently released from the sediments for the whole duration of the flow-through column experiments (Fig. S4A). In contrast, in the pH 3 systems (+PO_4 and -PO_4), Na concentrations were not significantly different from that of the influent solution (Fig. S4G). High K concentrations were released from both +PO_4 and -PO_4 systems during the first 50 PV irrespective of weathering pH (Fig. S4B and S4H). Conversely, Ca and Mg from the influent solutions were immobilized in the sediments during the same initial 50 PV period (Figs. S4C, S4D, S4I and S4J). In the pH 2, +PO_4, 180 d systems, calculated moles of K^+ charge released from the sediments during the first 50 PV (*ca.* 2200 μmol_c), were similar to the sum of retained charge for Mg and Ca (*ca.* 2500 μmol_c). Similar results were observed for the other systems, consistent with $K^+ \rightarrow Mg^{2+}$ and $K^+ \rightarrow Ca^{2+}$ exchange reactions. Whereas sulfate release did not appear to be affected by the presence or absence of PO_4 in the acidic waste weathering solutions, they were affected by pH; net sulfate release was observed from the pH 2 weathered sediments, but not from pH 3 systems, where effluent sulfate concentrations dropped substantially below the influent solution value after 800 PV (Fig. S4F and S4L).

LCFs of the U L_{III}-edge EXAFS spectra obtained after the BPW flow-through column experiments indicated in the -PO_4 sediment systems at pH 2 the presence of phosphuranylite (365 d: 68%), boltwoodite (365 d: 27%), and meta-ankoleite (365 d: 17%). Boltwoodite (365 d: 41%), phosphuranylite (365 d: 35%), and becquerelite (180 d: 24%) were detected in the pH 3 systems. In the +PO_4 systems at pH 2, meta-ankoleite (365 d: 55%) and boltwoodite (365 d: 30%) were the major phases with smaller becquerelite (365 d: 15%) and schoepite (365 d: 15%) contributions. At pH 3, schoepite (365 d: 23%), meta-ankoleite (365 d: 21%) and boltwoodite (365 d: 19%) showed similar contribution to the LCF fit, whereas meta-ankoleite was the main phase (365 d: 40%).

3.3. Equilibrium speciation modeling

For the pH 2, -PO_4 systems, effluent solutions were near saturation with respect to meta-ankoleite and autunite $[Ca(UO_2)_2(PO_4)_2]$ (Fig. 3A and B). However, in the pH 3, -PO_4 systems, the log Ω values for autunite were supersaturated after 800 PV (Fig. 3C and D). Effluent solutions in the pH 3 and 180 d, +PO_4 systems were slightly oversaturated with respect to autunite (Fig. 3G), but near equilibrium with meta-ankoleite.

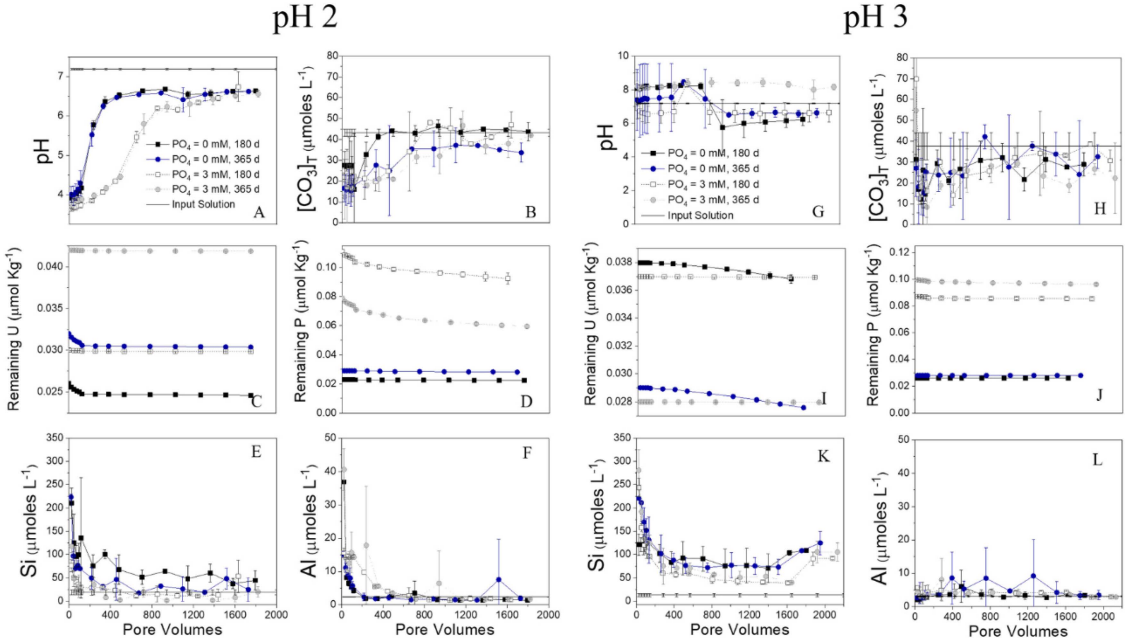

Fig. 2. Evolution (in pore volumes) of effluent solution chemistry (pH – A, G; total dissolved carbonate – B, H; Si – E, K; Al – F, L) and remaining U and P content (as the cumulative release from initial concentration; C, I and D, J, respectively) of acidic waste-weathered Hanford sediments (PO_4-reactant and PO_4-reactant free systems at pH 2 or 3, after 180 or 365 days) leached in flow-through columns with a background porewater (BPW) solution (pH 7.2). Error bars represent 95% confident interval. Solid lines (without symbols) indicate influent concentrations in BPW.

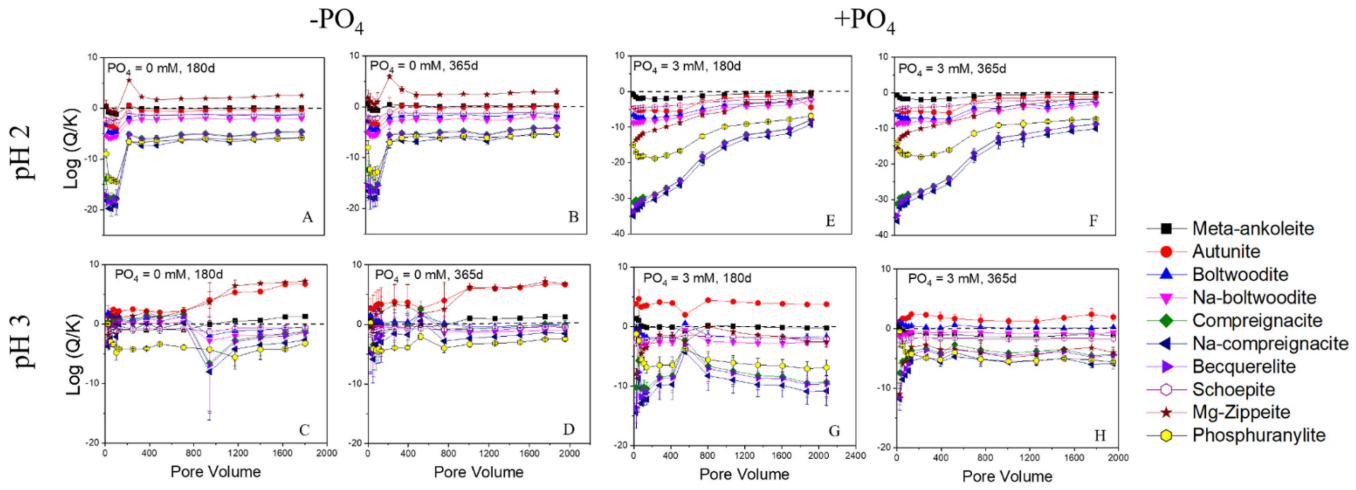

Fig. 3. Evolution (in pore volumes) of mineral saturation indices (as log(Q/K)) in effluent solutions of acidic waste-weathered Hanford sediments (PO_4-reactant (+PO_4) and PO_4-reactant free (-PO_4) systems at pH 2 or 3, after 180 or 365 days) leached in flow-through columns with a background porewater (BPW) solution (pH 7.2). Error bars represent one standard deviation of duplicated columns measurements. Mineral solubility constants considered in speciation calculations are reported in Table S7-S14. The saturation indices calculated and presented in this figure labeled phosphuranylite correspond to $K_4[(UO_2)_3O_2(PO_4)_2]$, a member of the phosphuranylite group.

Solutions were not supersaturated with respect to either of these two phases in the pH 2, +PO4 systems (Fig. 3E and F). The effluent solutions from all pH 2 systems were slightly undersaturated with respect to uranyl silicate minerals (boltwoodite and Na-boltwoodite) but presented a greater solution phase undersaturation for uranyl (oxy)hydroxide minerals (compreignacite, Na-compreignacite, and becquerelite), an effect that was amplified for sediments weathered in the presence of PO_4 (Fig. 3A-B, E-F). The -PO_4 sediments (pH 2 and 3) produced effluent solutions that were supersaturated with respect to Mg-zippeite after 200 PV (Fig. 3A-B), and near saturation with respect to all uranyl phosphate, (oxy)hydroxide and silicate minerals during the first 800 PV, followed by undersaturation for the remaining length of the experiment.

Effluent solutions were generally undersaturated with respect to $K_4[(UO_2)_3O_2(PO_4)_2]$, a K-bearing endmember of the phosphuranylite group (Fig. 3; numerical values given in Tables S7–S14, Supplemental Information). Exceptions were observed during the first 30 pore volumes in -PO_4 systems at pH 3 (180 d and 365 d). Importantly, this member has a different stoichiometry than the Ca-bearing phosphuranylite phase identified in the flow-through sediments by EXAFS ($KCa(H_3O)_3(UO_2)_7(PO_4)_4O_4 \cdot 8\ H_2O$). In addition to the presence of Ca, the EXAFS reference has a UO_2 to PO_4 ratio of 3.5–2 in addition to 8 moles of structural water and 3 moles of H_3O^+; whereas, $K_4[(UO_2)_3O_2(PO_4)_2]$ has a UO_2 to PO_4 ratio of 3–2 and is anhydrous. The EXAFS results and our prior study of uranyl phosphate alteration and dissolution (Reinoso-Maset et al., 2020) suggest that the phosphuranylite member formed in the flow-through experiments contains both K and Ca between uranyl-phosphate structural layers, which is also consistent with the much higher Ca relative to K concentration in column effluents (Fig. S4).

In -PO_4 systems at pH 2, aqueous speciation calculations indicate that uranyl cation UO_2^{2+} and UO_2OH^+ were the dominant species in effluent solutions of all systems during the first 400 PV, followed by a significant, gradual increase in predominance of $Ca_2UO_2(CO_3)_3$, $UO_2(CO_3)_2^{2-}$, and $CaUO_2(CO_3)_3^{2-}$ (Fig. S5, Supplemental Information). In -PO_4 systems at pH 3, $(UO_2)_2CO_3(OH)_3$ was the predicted dominant species (Fig. S5, Supplemental Information).

4. Discussion

4.1. Role of phosphate on U retention in acidic waste-weathered sediments

It is known that dissolved phosphate was a periodic component of acidic U-bearing waste discharged into the vadose zone at the Hanford site, but the precise concentration and frequency of its presence are poorly known. The results of this study indicate that the presence of dissolved phosphate as a waste component impacted the speciation of U incorporated into the sediments. Specifically, in the presence of phosphate (*i.e.*, +PO_4 systems), a large fraction of waste-derived U precipitated as meta-ankoleite at both pH 2 and 3 (Fig. 4; Perdrial et al., 2018). Meta-ankoleite also formed in the absence of added phosphate (*i.e.*, -PO_4 systems), but only under pH 2 conditions (Fig. 4). This pH effect in -PO_4 systems can be attributed to the positive impact of proton concentration on the dissolution of native PO_4-bearing minerals (*e.g.*, apatite) in the Hanford sediments. The more acidic conditions (pH 2) might have promoted a greater release of phosphate, promoting the formation of meta-ankoleite by precipitation with uranyl cations present in the weathering solution. Conversely, the pH 3, -PO_4 weathering reaction provided insufficient phosphate to promote meta-ankoleite precipitation and thus the formation of compreignacite, a non-PO_4-bearing phase, was favored (Fig. 4). Additionally, proton-promoted dissolution of native silicates resulted in the formation of Si-bearing phases such as boltwoodite in all treatments, but with a greater prevalence in the pH 2 systems (Fig. 4, Perdrial et al., 2018). No major differences in the main mineral components were observed due to the weathering time, with exception of becquerelite, which had higher prevalence at 185 d than after 365 d (Fig. 4), suggesting an apparent meta-stable precipitate. Overall, the presence of PO_4 in the weathering solution resulted in a higher retention in the form of uranyl phosphate minerals.

4.2. Effect of solid phase speciation on subsequent U release

The primary purpose of this study was to determine the impact of variable weathering conditions on the subsequent lability and release of U retained in acidic waste-weathered sediments during leaching with a BPW solution. Although the extractability (Fig. 1) and solid phase speciation (Fig. 4) of U varied significantly between weathering treatments, the total U incorporated in neoformed phases remained unchanged. This allowed to assess the impact of the initial U solid phase speciation (*i.e.*, post-weathering) on (1) the extent of U solubilization and release from the weathered sediments (Figs. 2) and (2) the transformation of U-bearing minerals as promoted by leaching with BPW (Fig. 4B). These two processes are inextricably linked because mineral transformations are known to exert a strong control on U release during BPW infusion (Reinoso-Maset et al., 2017, 2020).

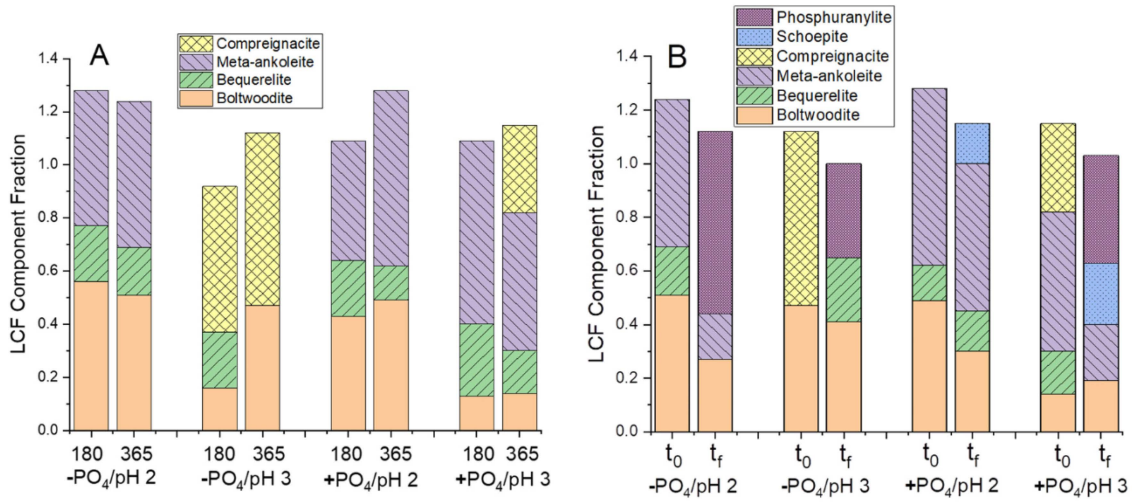

Fig. 4. Results of linear combination fits (LCF) of U L_{III}-edge EXAFS spectra for acidic waste-weathered Hanford sediments (fine fractions) before (A; *i.e.*, reacted with and without phosphate, at pH 2 or 3, for 180 or 365 d) and after (B) BPW flow-through column experiments. (A) shows the effect of waste-weathering treatment on the U solid phase speciation, whereas (B) shows the U speciation change resulting from BPW leaching of the 365 d weathered samples (t_0 = end of weathering, t_f, = end of leaching). Component fractions were obtained using spectra of uranyl reference compounds. Fraction values and sum errors are given in Table S2, Supplemental Information. EXAFS LCF for the pH 3 weathered sediments at the end of weathering were obtained from Perdrial et al. (2018). The LCF obtained from U L_{III}-edge EXAFS spectra and presented in this figure correspond to phosphuranylite, $KCa(H_3O)_3(UO_2)_7(PO_4)_4O_4 \cdot 8\ H_2O$.

Solid phases controlling U release in the -PO_4 systems were strongly dependent on pH. After BPW leaching, the boltwoodite-like, becquerelite-like, and meta-ankoleite-like phases decreased in the pH 2, -PO_4, 365 d weathered sediments, but a phosphuranylite-like phase appeared (Fig. 4B). This system also released the largest mass of U among the four 365 d treatments (Fig. 2C). However, it is noteworthy that most of the mass loss of U occurred during the first 80 PV of BPW leaching (Fig. 2C), when effluent solutions were most undersaturated with respect to boltwoodite and becquerelite, whereas solutions were near equilibrium with meta-ankoleite (Fig. 3B). Hence, boltwoodite and becquerelite dissolution was greatest early in the experiment, favoring the release of associated U into the effluent.

Leaching of the pH 3, -PO_4, 365 d weathered sediments was initiated with a similar mass fraction of boltwoodite as in the pH 2 systems but these sediments contained *ca.* half of the U in a compreignacite-like phase instead of meta-ankoleite and becquerelite (Fig. 4B). Effluent solutions from this system never achieved undersaturation with respect to boltwoodite (Fig. 3D), which is consistent with the very small variation observed in the EXAFS LCF for this phase (Fig. 4B). Solutions were undersaturated with respect to compreignacite, particularly during the first 200 PV (Fig. 3D). Compreignacite-like phases were not detectable at the end of the experiment and had been largely replaced with becquerelite- and phosphuranylite-like minerals (Fig. 4B). These results suggest that the low U release at an early stage was due to incongruent dissolution of the uranyl oxyhydroxides such as compreignacite (Reinoso-Maset et al., 2017) and the subsequent, rather rapid transformation to, or precipitation of, a phosphuranylite-type phase (Kanematsu et al., 2014) due to the release of the PO_4 present in unreacted Hanford sediments (Table S1).

With the inclusion of phosphate in the waste weathering solution (+PO_4 systems), meta-ankoleite became an important component of the initial U speciation in the sediments. The pH 2, +PO4, 365 d sediments showed a significant loss of U from boltwoodite-like phases, as reflected by the EXAFS LCFs before and after leaching (Fig. 4B) and the undersaturation of the effluent solution with respect to this phase (Fig. 3E–F). Conversely, despite undersaturation with respect to becquerelite (Fig. 3E-F), the relative fraction of this phase remained unchanged during the BPW infusion for 2000 PV (Fig. 4B). Effluent solutions remained near equilibrium saturation with respect to meta-ankoleite (Fig. 3E–F) thus little to no reduction in the relative fraction of meta-ankoleite-like phases was observed after leaching (Fig. 4B); whereas the increase of schoepite-like U phases (Fig. 4B) is consistent with the effluent BPW approaching equilibrium conditions for that specific phase (Fig. 3E–F).

For the pH 3 systems, compreignacite was an important component of U speciation that was removed during leaching (Fig. 4B), consistent with the large undersaturation of effluent BPW with respect to this phase (Fig. 3H). Effluent solutions from these systems were also slightly undersaturated with respect to meta-ankoleite (Fig. 3H), likely decreasing the fraction of that component in the LCFs of post-reaction sediment spectra (Fig. 4B). However, two factors appear to have limited the release of U from these columns (as reflected in the non-detectable change in solid phase U; Fig. 2I). First, the leaching solutions remained near equilibrium or slightly supersaturated with respect to boltwoodite, which maintained the stability of that phase during the leaching experiments. Second, the formation of schoepite-like and phosphuranylite-like phases that incorporated U released by the dissolution (or conversion) of compreignacite and meta-ankoleite. Kanematsu et al. (2014) observed the transformation of meta-ankoleite to a phosphuranylite-type phase due to Ca substitution in the mineral structure. Initial uptake in Ca by the sediments is consistent with this effect (Fig. S4I).

Our EXAFS LCF results indicated the neoformation of a phosphuranylite-like phase (ideal stoichiometry $KCa(H_3O)_3(UO_2)_7(PO_4)_4O_4 \cdot 8\ H_2O$). However, the calculated saturation indices for the phosphuranylite-group member $K_4[(UO_2)_3O_2(PO_4)_2]$ indicated that most effluent solutions were undersaturated with respect to this mineral. This discrepancy can be attributed to differences in UO_2 to PO_4 ratio, structural water, and Ca content. For instance, the identified EXAFS mineral most likely contains interlayer Ca and K, whereas, the reported uranyl-phosphate species in Juillerat et al. (2018) contains only K. Comparison of solubilities among uranyl silicate, oxyhydroxide, and phosphate groups suggests that the presence of Ca and interlayer water will increase solubility (per uranyl cation) for similar mineral structures (Chen et al., 1999; Shvareva et al., 2012), but the much higher Ca concentration in effluent solutions (Fig. S4) likely counteracted that effect in the current experiments, promoting oversaturation of solutions with respect to the Ca-bearing phosphuranylite phase. The limitation on available thermodynamic data for phosphuranylite-type phases prompts the need to conduct calorimetric and solubility experiments to measure

the Gibbs free energy (ΔG^0_f) and enthalpy (ΔH^0_f) of formation for minerals in this group with known stoichiometry and structure. Reliable and accurate thermodynamic information on uranyl phosphate minerals is crucial to provide plausible remediation strategies to attenuate U(VI) mobilization in contaminated sites.

5. Implications for U(VI) mobilization in the hanford vadose zone

Results obtained from *in-situ* characterization, synthetic acidic weathered batch and leaching experiments suggest that if phosphate was present in acidic waste disposed of at the Hanford Site, a large mass fraction of U(VI) would be precipitated as uranyl-phosphate phases (McKinley et al., 2007; Kanematsu et al., 2014; Gartman et al., 2015; Wang et al., 2017; Perdrial et al., 2018). The neo-formation of uranyl-phosphates would retard the transport of U(VI) into groundwater and contribute to the long-term immobilization of U(VI) in the vadose zone. Studies on the extent of uranyl partitioning into Hanford sediments exposed to synthetic acidic waste suggested that uranyl-phosphates (*e.g.*, meta-autunite and phosphuranylite group) formed in the sediments reacted with solutions containing phosphate (Gartman et al., 2015; Perdrial et al., 2018). Our experiments revealed that upon leaching with circumneutral BPW, sediments weathered under acidic conditions and in the presence of dissolved phosphate released little to no U to the effluent solution, an observation attributable to the presence of uranyl-phosphate minerals, in particular meta-ankoleite. On the other hand, in the absence of phosphate, *ca.* 5% of U was released due to the dissolution of becquerelite, bolwoodite, and compreignacite, similar to results observed by Wang et al. (2017). Our results also revealed complex uranyl-bearing transformations occurring during BPW leaching. Upon contact with the circumneutral BPW, the solid phase U speciation changed, suggesting the potential transformation of meta-ankoleite into a phosphuranylite-type phase through incorporation of Ca and becquerelite into schoepite from loss of Ca. While it is unclear whether these transformations occur *via* ion exchange or dissolution/re-precipitation process, the implications for U fate and transport in systems where pH fluctuates upon contaminant source removal are important.

CRediT authorship contribution statement

Jon Chorover and Nicolas Perdrial: Conceptualization, **Jon Chorover:** Funding acquisition, Project administration, Resources, Supervision, **Angélica Vázquez-Ortega:** Methodology, Investigation, Data curation, Formal analysis, Validation, Visualization, Writing - original draft, **All authors:** Writing - review & editing.

Declaration of Competing Interest

The authors declare that they have no known competing financial interests or personal relationships that could have appeared to influence the work reported in this paper.

Acknowledgments

Special thanks to Mary Kay Amistadi, Alex Chacara, Kris Ford, Masakazu Kanematsu, Michael Pohlmann, Robert Root, and Patrick Broxton. This research was funded by the Subsurface Biogeochemical Research (SBR) Program, Biological and Environmental Research (BER), Office of Science, U.S. Department of Energy (grant number SBR-DE-SC0006781). Portions of this research were carried out at the Stanford Synchrotron Radiation Lightsource, a national user facility operated by Stanford University on behalf of the U.S. Department of Energy, Office of Basic Energy Sciences.

Appendix A. Supporting information

Supplementary data associated with this article can be found in the online version at doi:10.1016/j.jhazmat.2021.126240.

References

Begin, L., Fortin, J., 2003. Evaluation of an acid ammonium oxalate extraction to determine fluoride resident concentrations in soils. J. Environ. Qual. 32 (2), 662–673.
Catalano, J.G., Heald, S.M., Zachara, J.M., Brown, G.E., 2004. Spectroscopic and diffraction study of uranium speciation in contaminated vadose zone sediments from the Hanford site, Washington state. Environ. Sci. Technol. 38 (10), 2822–2828.
CH2M HILL, 2010. Data Quality Objectives Summary Report for the Uranium Sequestration Pilot Test SGW-46487. Richland,, Washington.
CH2M HILL, 2006. Hanford Soil Inventory Model (SIM) Rev. 1 Users Guide.
Chen, F., Ewing, R.C., Clark, S.B., 1999. The Gibbs free energies and enthalpies of formation of U^{6+} phases: an empirical method of prediction. Am. Miner. 84, 650–664.
Chorover, J., Choi, S., Rotenberg, P., Serne, R.J., Rivera, N., Strepka, C., Thompson, A., Mueller, K.T., O'Day, P.A., 2008. Silicon control of strontium and cesium partitioning in hydroxide-weathered sediments. Geochim. Et. Cosmochim. Acta 72 (8), 2024–2047.
Christensen, J.N., Dresel, P.E., Conrad, M.E., Maher, K., Depaolo, D.J., 2004. Identifying the sources of subsurface contamination at the Hanford Site in Washington using high-precision uranium isotopic measurements. Environ. Sci. Technol. 38 (12), 3330–3337.
Corbin, R.A., Simpson, B.C., Anderson, M.J., Danielson, W.F., Field, J.G., Jones, T.E., Kincaid, C.T., 2005. Hanford soil inventory model. Review 1. RPP-26744.
DOE, U.S., 2010. 216-U-8 Crib and 216-U-12 crib vadose zone characterization sampling and analysis plan. Dep. Energy.
Dold, B., 2003. Speciation of the most soluble phases in a sequential extraction procedure adapted for geochemical studies of copper sulfide mine waste. J. Geochem. Explor. 80 (1), 55–68.
Gartman, B.N., Qafoku, N.P., Szecsody, J.E., Kukkadapu, R.K., Wang, Z., Wellman, D.M., Truex, M.J., 2015. Uranium fate in Hanford sediment altered by simulated acid waste solutions. Appl. Geochem. 63, 1–9.
Gorman-Lewis, D., Fein, J.B., Burns, P.C., Szymanowski, J.E.S., Converse, J., 2008. Solubility measurements of the uranyl oxide hydrate phases metaschoepite, compreignacite, Na-compreignacite, becquerelite, and clarkeite. J. Chem. Thermodyn. 40 (6), 980–990.
Juillerat, C.A., Moore, E.E., Kocevski, V., Besmann, T., zur Loye, H., 2018. A family of layered phosphates crystallizing in a rare geometrical isomer of the phosphuranylite topology: synthesis, characterization, and computational modeling of A(4)[(UO2)(3)O-2(PO4)(2)] (A = Alkali Metal) exhibiting intralayer ion exchange. Inorg. Chem. 57 (8), 4726–4738.
Kanematsu, M., Perdrial, N., Um, W., Chorover, J., O'Day, P.A., 2014. Influence of phosphate and silica on U(VI) precipitation from acidic and neutralized wastewaters. Environ. Sci. Technol. 48 (11), 6097–6106.
Lussier, A.J., Lopez, R.A.K., Burns, P.C., 2016. A revised and expanded structure hierarchy of natural and synthetic hexavalent uranium compounds. Can. Mineral. 54, 177–283.
McKeague, J.A., Day, D.H., 1966. Dithionite- and oxalate-extractable Fe and Al as aids in differentiating various classes of soils. Can. J. Soil Sci. 46 (1), 13–22, 13-&.
McKinley, J.P., Zachara, J.M., Wan, J., McCready, D.E., Heald, S.M., 2007. Geochemical controls on contaminant uranium in vadose Hanford formation sediments at the 200 area and 300 area, Hanford Site, Washington. Vadose Zone J. 6 (4), 1004–1017.
Mehta, V.S., Maillot, F., Wang, Z., Catalano, J.G., Giammar, D.E., 2016. Effect of reaction pathway on the extent and mechanism of uranium(VI) immobilization with calcium and phosphate. Environ. Sci. Technol. 50 (6), 3128–3136.
Mehta, V.S., Maillot, F., Wang, Z., Catalano, J.G., Giammar, D.E., 2014. Effect of co-solutes on the products and solubility of uranium (VI) precipitated with phosphate. Chem. Geol. 364, 66–75.
Pan, Z., Giammar, D.E., Mehta, V., Troyer, L.D., Catalano, J.G., Wang, Z., 2016. Phosphate-Induced Immobilization of Uranium in Hanford Sediments. Environ. Sci. Technol. 50 (24), 13486–13494.
Perdrial, N., Vazquez-Ortega, A., Wang, G., Kanematsu, M., Mueller, K.T., Um, W., Steefel, C.I., O'Day, P.A., Chorover, J., 2018. Uranium speciation in acid waste-weathered sediments: the role of aging and phosphate amendments. Appl. Geochem. 89, 109–120.
Reinoso-Maset, E., Perdrial, N., Steefel, C.I., Um, W., Chorover, J., O'Day, P.A., 2020. Dissolved carbonate and pH control the dissolution of uranyl phosphate minerals in flow-through porous media. Environ. Sci. Technol. 54, 6031–6042.
Reinoso-Maset, E., Steefel, C.I., Um, W., Chorover, J., O'Day, P.A., 2017. Rates and mechanisms of uranyl oxyhydroxide mineral dissolution. Geochim. Et. Cosmochim. Acta 207, 298–321.
Riley, R.G., Zachara, J.M., 1992. Chemical contaminants on DOE lands and selection of contaminant mixtures for subsurface science research. Off. Energy Res. Subsurf. Sci. Program, U. S. DOE.
Shvareva, T.Y., Fein, J.B., Navrotsky, A., 2012. Thermodynamic properties of uranyl minerals: constraints from calorimetry and solubility measurements. Ind. Eng. Chem. Res. 51, 607–613.

Thompson, A., Steefel, C.I., Perdrial, N., Chorover, J., 2010. Contaminant desorption during long-term leaching of hydroxide-weathered hanford sediments. Environ. Sci. Technol. 44 (6), 1992–1997.

Um, W., Wang, Z., Serne, R.J., Williams, B.D., Brown, C.F., Dodge, C.J., Francis, A.J., 2009. Uranium phases in contaminated sediments below Hanford's U Tank farm. Environ. Sci. Technol. 43 (12), 4280–4286.

Wang, G., Um, W., Wang, Z., Reinoso-Maset, E., Washton, N.M., Mueller, K.T., Perdrial, N., O'Day, P.A., Chorover, J., 2017. Uranium release from acidic weathered Hanford sediments: single-pass flow-through and column experiments. Environ. Sci. Technol. 51 (19), 11011–11019.

Zachara, J.M., Brown, C.F., Christensen, J.N., Davis, J.A., Dresel, P.E., Liu, C., Kelly, S.D., McKinley, J.P., Serne, R.J., Um, W., 2007. A site wide perspective on uranium geochemistry at the hanford site. A site wide perspective uranium. Geochem. Hanford Site.

Zhou, P., Gu, B.H., 2005. Extraction of oxidized and reduced forms of uranium from contaminated soils: Effects of carbonate concentration and pH. Environ. Sci. Technol. 39 (12), 4435–4440.